CHALMERS
UNIVERSITY OF TECHNOLOGY

Multiscale X-ray imaging and characterisation of pharmaceutical dosage forms

International Journal of Pharmaceutics 642 (2023) 123200

Contents lists available at ScienceDirect

International Journal of Pharmaceutics

journal homepage: www.elsevier.com/locate/ijpharm

Multiscale X-ray imaging and characterisation of pharmaceutical dosage forms

Martina Olsson [a], Rydvikha Govender [b,c], Ana Diaz [d], Mirko Holler [d], Andreas Menzel [d], Susanna Abrahmsén-Alami [e], Matthew Sadd [a], Anette Larsson [c,f], Aleksandar Matic [a,f,g,*], Marianne Liebi [a,d,h,*]

[a] Department of Physics, Chalmers University of Technology, SE-412 96 Gothenburg, Sweden
[b] Oral Product Development, Pharmaceutical Technology and Development, Operations, AstraZeneca, SE-431 83 Mölndal, Sweden
[c] Department of Chemistry and Chemical Engineering, Chalmers University of Technology, SE-412 96, Gothenburg, Sweden
[d] Photon Science Division, Paul Scherrer Institut, Villigen PSI, 5232, Switzerland
[e] Innovation Strategies & External Liaison, Pharmaceutical Technology & Development, Operations, AstraZeneca, SE-431 83 Mölndal, Sweden
[f] FibRe-Centre for Lignocellulose-based Thermoplastics, Department of Chemistry and Chemical Engineering, Chalmers University of Technology, SE-412 96 Gothenburg, Sweden
[g] Wallenberg Wood Science Center, Chalmers University of Technology, SE-412 96 Gothenburg, Sweden
[h] Institute of Materials, École Polytechnique Fédérale de Lausanne (EPFL), Lausanne 1015 Switzerland

ARTICLE INFO

Keywords:
Ptychographic X-ray computed nanotomography
Scanning SAXS/WAXS
μXRD
Solid dispersion
Carbamazepine

ABSTRACT

A correlative, multiscale imaging methodology for visualising and quantifying the morphology of solid dosage forms by combining ptychographic X-ray computed nanotomography (PXCT) and scanning small- and wide-angle X-ray scattering (S/WAXS) is presented. The methodology presents a workflow for multiscale analysis, where structures are characterised from the nanometre to millimetre regime. Here, the method is demonstrated by characterising a hot-melt extruded, partly crystalline, solid dispersion of carbamazepine in ethyl cellulose. Characterisation of the morphology and solid-state phase of the drug in solid dosage forms is central as this affects the performance of the final formulation. The 3D morphology was visualised at a resolution of 80 nm over an extended volume through PXCT, revealing an oriented structure of crystalline drug domains aligned in the direction of extrusion. Scanning S/WAXS showed that the nanostructure is similar over the cross section of the extruded filament, with minor radial changes in domain sizes and degree of orientation. The polymorphic forms of carbamazepine were qualified with WAXS, showing a heterogeneous distribution of the metastable forms I and II. This demonstrates the methodology for multiscale structural characterization and imaging to enable a better understanding of the relationships between morphology, performance, and processing conditions of solid dosage forms.

1. Introduction

Efficient delivery of the drug substance is essential to achieve and maintain the intended therapeutic effect of a medication. Oral drug delivery is the most common route due to ease of administration, cost-effectiveness, and high patient compliance, but it also sets requirements on the dosage form to preserve the functionality of the drug throughout the biological system, e.g., dissolution in gastrointestinal fluids (Liu et al., 2015). Consequently, the formulation needs to ensure that the intended therapeutic effect is reached by controlling the drug distribution, by stabilising the intended solid-state phase of the drug, and reaching the target drug release profile.

For solid dosage forms, structure and morphology often play a critical role in establishing the performance of the drug delivery system. Solid dispersions are one example where the drug is dispersed in a stabilising polymeric carrier to improve the solubility of the drug (Govender et al., 2020; Pandi et al., 2020; Schittny et al., 2020). Here, the extent of mixing between the drug and the polymer is critical to

Abbreviations: PXCT, ptychographic X-ray computed nanotomography; S/WAXS, small- and wide-angle X-ray scattering; DSC, differential scanning calorimetry; XRD, X-ray diffraction.

* Corresponding authors at: Department of Physics, Chalmers University of Technology, SE-412 96 Gothenburg, Sweden.
E-mail addresses: matic@chalmers.se (A. Matic), marianne.liebi@psi.ch (M. Liebi).

https://doi.org/10.1016/j.ijpharm.2023.123200
Received 1 May 2023; Received in revised form 30 June 2023; Accepted 1 July 2023
Available online 4 July 2023

hinder phase transformation or recrystallisation and degraded performance both during storage and dissolution (Baghel et al., 2016). Pharmaceutical coatings are another example where the morphology can be used as a direct method for controlled release and the connectivity, tortuosity and domain size are directly linked to the release rate (Habel et al., 2016; Marucci et al., 2013). A third example are solid dosage forms prepared for preserving a specific polymorph of a drug where the solid-state phase is of importance, e.g. for formulations presenting large variations in dissolution characteristics for different polymorphs (Florence, 2010; Sanabria Ortiz et al., 2019). Moreover, the selected processing method for the dosage form can have a large impact on structures formed during the preparation step. One manufacturing process that continues to grow in importance for solid dispersions in pharmaceutical industry is hot-melt extrusion, where the raw materials are fed into a heated barrel containing a single or two rotating screws (Alzahrani et al., 2022; Butreddy et al., 2021; Deshmukh et al., 2020; Repka et al., 2018; Tiwari et al., 2016). The exposure to the heat from the barrel and the shear and elongational forces from the rotating screws melt, mix and convey the material towards a die where it is ejected. Depending on the processing conditions, structures and heterogeneities may form in this process, which can have an impact on the properties of the formulation (Duan et al., 2020). To be able to engineer and optimise the performance of solid dosage forms, it is important to understand the connection between performance and morphology, and how it relates to the preparation process. A first step in establishing this is to characterise the morphology in depth across multiple length scales to provide insight into how it relates to important properties of the formulation such as physical stability and release rate.

A wide variety of analytical techniques have traditionally been used to investigate heterogeneities and determine the solid-state phase in pharmaceutical dosage forms. These include differential scanning calorimetry (DSC) (Baird & Taylor, 2012), powder X-ray diffraction (PXRD) (Rumondor et al., 2009; Takeuchi et al., 2015), solid state nuclear magnetic resonance (ssNMR) (Lefort et al., 2004; Pindelska et al., 2015), infrared (IR) (Rumondor & Taylor, 2010), and Raman spectroscopy (Luebbert et al., 2018). These techniques can all capture the state of the drug and shed some light on mixing and de-mixing. Yet, to fully understand the morphological properties and their impact on product performance, there is a need for direct visualisation over extended sample volumes. However, imaging of pharmaceutical formulations can be challenging as the density and chemistry of the components are often similar, which creates difficulties in obtaining sufficient contrast. Invasive characterisation methods, such as fluorescence spectroscopy with fluorescence agents, or partial leaching of specific phases (Fager et al., 2020a; Purohit et al., 2017; Purohit & Taylor, 2015, 2017; Tian et al., 2016), can be used to enhance the contrast. However, this can induce changes to the solid-state phase and/or the morphology, which complicates the analysis. For three-dimensional imaging, focused ion beam - scanning electron microscopy (FIB-SEM) has been used for pharmaceutical coatings by consecutive imaging during serial sectioning (Fager et al., 2020a). FIB-SEM imaging provides high resolution, but the sectioning may introduce artefacts. In addition, the technique remains challenging for poorly conducting and soft materials, such as pharmaceutical formulations (Fager et al., 2020b).

Another useful three-dimensional characterisation technique is X-ray computed tomography, allowing for non-destructive imaging of the interior volume of a sample. This technique has been applied to solid dosage forms for non-destructive characterisation of the interior structure and morphology (Gamble et al., 2021; Vijayakumar et al., 2023) and for non-destructive identification of drug polymorphs in solid samples (Yamamoto et al., 2021). Ptychographic X-ray computed nanotomography (PXCT) is a tomography method based on image reconstruction from coherent X-ray scattering that provides an image of the quantitative electron density distribution in samples with diameters of tens of micrometres at resolutions approaching tens of nanometres (Dierolf et al., 2010; Pfeiffer, 2018). PXCT is a sensitive technique for resolving small contrast variations, which is especially important for soft or biological materials, such as pharmaceutical samples, which have small electron density variations. As an example, previous PXCT results have shown the capability of the method for distinguishing water and oil in food emulsions, resolving contrast variations as small as 0.04 e/Å^3 (Nielsen et al., 2016). For pharmaceutical applications PXCT have recently been used for quantifying the morphology and electron density of nanofibrillated cellulose hydrogels (Koivunotko et al., 2021) and aerogels (Merivaara et al., 2022) reaching 3D resolutions of 80–120 nm.

In this study, PXCT is combined with scanning small- and wide-angle X-ray scattering (S/WAXS), the latter also known as μXRD, to establish a workflow for multiscale characterisation for evaluating structure and morphology of solid dosage forms in three dimensions. Scanning S/WAXS is an imaging method where a focused X-ray beam is used to spatially resolve the scattering of a sample. With this technique, a sample is scanned through the focused beam, collecting a scattering pattern in each scan point in order to derive information on the nanostructure distribution over a sample (Arboleda et al., 2019; Giannini et al., 2014; Rodriguez-Palomo et al., 2021). The methodology is here applied to a partly crystalline solid dispersion of carbamazepine in ethyl cellulose prepared through hot-melt extrusion to demonstrate the capability of spatially resolving the distribution and composition of different phases in the sample and determining the polymorphic form of the drug. Fig. 1a and b shows a schematic overview of the two techniques and examples of analysis results obtained from them in this work. To be able to use the combination of PXCT and scanning S/WAXS in a correlative manner, it is necessary that there is an overlap between the length scale probed by SAXS (1–500 nm) and the resolution of the nanotomography (80 nm). This enables a direct correlation between the morphology revealed with nanotomography and the statistical information on nanostructures probed by SAXS. An overlap is also set between the beam and step size in the scanning S/WAXS (25 μm), and the volume imaged in the nanotomography (d = 50 μm). This approach bridges the length scales investigated by the two methods, as illustrated in Fig. 1c, and enable a multiscale characterisation from the nanometre to millimetre scale.

2. Methods

2.1. Preparations of melt extruded filaments

Carbamazepine was obtained from AstraZeneca, ethyl cellulose (Ethocel^{TM} Standard 45 Premium) was supplied by Dow. Carbamazepine powder and ethyl cellulose powder were physically mixed in a 5 g batch with 50% w/w carbamazepine content. The mixture was fed via a hopper into the barrel of a 5 mL capacity Xplore micro compounder (Xplore Instruments BV) with two co-rotating conical mixing screws and a circular die of 1.5 mm in diameter. The barrel temperature was set to 180 °C to be well above the glass transition temperature of the polymer while low enough not to induce thermal degradation. A neat ethyl cellulose filament was extruded at a temperature of 150 °C as a reference. Prior to the X-ray measurements the extruded filaments were stored under ambient conditions for 1 month.

2.2. Differential scanning calorimetry (DSC)

DSC measurements were carried out using a TA Q1000 instrument. A piece of the filament (~5 mg) was weighed and put in a hermetically sealed aluminium pan. An empty pan was used as a reference. Helium and nitrogen were used as purge gases for the sample chamber at a flow rate of 50 mL/min. All samples were initially cooled to 0 °C and measured by heating to 200 °C, 2 min isotherm at 200 °C, cooling to 0 °C, 2 min isotherm at 0 °C, followed by a second heating step to 200 °C. The heating and cooling rates were kept at 10 °C/min.

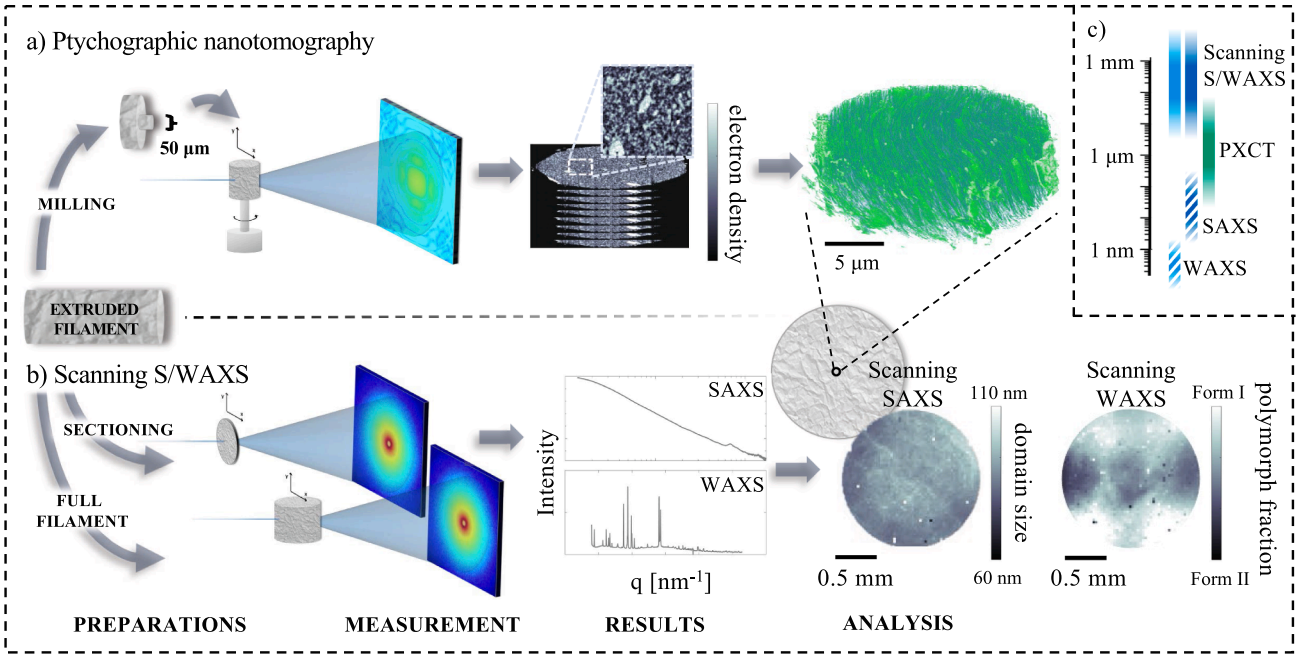

Fig. 1. Schematic diagram of the correlative X-ray imaging methodology with combined PXCT and scanning S/WAXS applied to an extruded filament, demonstrating the steps from sample preparation and experimental setup to results. a) For PXCT the extruded filament is prepared as a small cylinder and measured with ptychographic tomography as explained in detail in section 2.3. From this, the three-dimensional electron density distribution is reconstructed, and morphological properties such as domain size and connectivity can be retrieved. b) For scanning S/WAXS, the entire extruded filament is sectioned in thin slices as well as measured over an intact piece of filament. With a scanning procedure, the scattering from the sample is spatially resolved over the full field of view of the filament. Each scattering pattern is analysed to generate an image where each pixel represents a property derived from the scattering pattern, such as domain size or dominating polymorphic form. c) Length scales covered by the described experimental methods, bridging the analysis of structures from sub-nanometre to millimetre scale. The lower, hatched S/WAXS scalebars represent the length scale of the structure and morphology characterised by the individual scattering techniques while the full, upper scalebars represent the scale of the imaging of these characteristics by the scattering techniques.

2.3. Ptychographic X-ray computed nanotomography (PXCT)

PXCT is a quantitative, high-resolution imaging technique that combines the phase reconstruction method of ptychography with tomographic imaging to resolve the electron density distribution in three dimensions (Dierolf et al., 2010). In X-ray ptychography, a confined, coherent illumination of typically a few microns is used to raster scan the sample in such a way that the illuminated areas partially overlap. At each scanning position, coherent diffraction patterns are recorded in the far field, and iterative phase retrieval algorithms are used to reconstruct the complex-valued transmissivity of the sample, with both phase and amplitude contrast (Pfeiffer, 2018). To prepare a 50 µm sized cylindrical sample of the carbamazepine dispersion needed for the PXCT, a lathe system, *Preppy*, developed at the cSAXS beamline, was used for mechanical milling (Holler et al., 2020). A small part of the extruded strand was glued to an OMNY pin (Holler et al., 2017) and a pillar was milled from the centre of the extruded strand. To protect the sample from elevated temperatures during milling, the drill was enclosed in a cryogenic chamber cooled by liquid nitrogen. The setup for the sample preparation is shown in Figure S1 in the supplementary information.

PXCT measurements were performed at the cSAXS beamline (X12SA) at the Swiss Light Source, Paul Scherrer Institut (Switzerland) under cryogenic conditions using the OMNY-setup (Holler et al., 2018), to mitigate structural changes caused by radiation damage. The illumination was defined on the sample with a photon energy of 6.2 keV using a coherently illuminated Fresnel zone plate with locally displaced zones, which makes an optimised illumination for ptychography (Odstrčil et al., 2019b). The beam size on the sample was about 8 µm and the flux was about 10^8 photons/s. Ptychographic scans were made over a field of view of 70 × 12 µm^2 (horiz × vert) with a step size of 2 µm to provide an overlap between neighbouring illuminated regions. At each scanning position diffraction patterns were collected with an acquisition time of 0.025 s with an in-vacuum Eiger 1.5 M detector. The detector was placed about 7.2 m downstream of the sample inside an evacuated flight tube. The ptychographic scans were collected at equally spaced angles from 0° to 180° generating 1600 projections for the tomographic reconstruction. The total acquisition time for this specimen was ~10 h, imparting a dose of ~1.2 × 10^7 Gy on the specimen, estimated as the surface dose assuming a material composition of $C_{20}H_{38}O_{11}$ (Howells et al., 2009). The absence of significant radiation damage was confirmed by the similarity of two reconstructed sub tomograms of the first and second half of the sampled dataset. PtychoShelves and the *cSAXS Matlab package* were used for ptychographic and tomographic reconstructions (Guizar-Sicairos et al., 2011; Odstrčil et al., 2019a; Wakonig et al., 2020). Ptychographic scans were reconstructed using the difference map algorithm (Thibault et al., 2009) followed by a maximum likelihood optimisation (Thibault & Guizar-Sicairos, 2012). The tomographic reconstruction was performed using a filtered back projection algorithm. The resolution was determined to 79 nm by Fourier shell correlation (FSC) using the half-bit criterion (van Heel & Schatz, 2005).

2.4. Image analysis of PXCT data

The reconstructed volumes were further processed in the image processing software ImageJ and Avizo. To reduce salt and pepper noise in the reconstructed tomogram a mean averaging filter with a kernel diameter of three pixels was applied in ImageJ. After filtering, segmentation was performed using interactive thresholding. Three phases were manually identified by the electron densities and morphology in the sample and were used to interactively set the threshold values for segmenting the three phases and from the processed image stack, 3D renderings were visualised using Avizo.

2.5. Scanning small- and wide-angle X-ray scattering (scanning S/WAXS)

SAXS and WAXS/XRD are statistical analysis techniques where the scattering signal of a sample is an average of all scatterer elements in the volume illuminated by the X-ray beam. SAXS can be interpreted using different models to extract information on nanostructures in the sample, whereas WAXS/XRD provides information in the Ångström length scale and thus provides information on degree of crystallinity as well as on the crystal structure, i.e., differentiation between polymorphs. In scanning S/WAXS, a focused X-ray beam is used to probe a smaller volume of the sample in each measurement, this technique is also known as micro-XRD. By also scanning the sample through the beam, the scattering of the sample is spatially resolved allowing for images to be created where each pixel contains the information from an individual scattering pattern from each scanning position (Bunk et al., 2009; Fratzl et al., 1997). To prepare the samples for scanning S/WAXS the extruded samples were embedded in epoxy and cut into 25 μm thin slices perpendicular to the direction of extrusion. The slices were cut with a thickness matching the step size of the scanning S/WAXS measurement so that each pixel in the scattering image originates from the scattering elements contained in a volume of 25 μm^3. The cross section was mounted using Kapton tape and an intact filament was directly attached to the sample holder to probe the scattering from both directions, perpendicular and parallel, to the extrusion direction (Fig. S2).

Scanning S/WAXS measurements were performed at the cSAXS beamline (X12SA) at the Swiss Light Source, Paul Scherrer Institut (Switzerland). The X-ray beam (photon energy of 11.2 keV) was focused to a spot size of approximately 25 × 25 μm^2. An evacuated flight tube was placed between the sample and the detectors to reduce air scattering and absorption. Scattering patterns were simultaneously measured using a Pilatus 2 M detector for SAXS and a Pilatus 300 k oriented as a vertical strip placed below the sample for WAXS with a sample to detector distance of approximately 7.1 m for SAXS and 0.6 m for WAXS. The samples were mounted on a motorised stage and scanned with a step size of 25 μm and an exposure time of 0.1 s.

2.6. Processing of scanning S/WAXS data

The two-dimensional scattering patterns were radially integrated to retrieve one-dimensional scattering curves with the *cSAXS scanning SAXS package* developed by the CXS group, Paul Scherrer Institut (Switzerland). The same package was used to perform orientational analysis (Bunk et al., 2009). Guinier analysis was used to fit the integrated SAXS curve to extract a characteristic size of drug domains in the polymer matrix by computing the radius of gyration, R_g. A combined Guinier-Porod model (Hammouda, 2010), was applied to fit the curve using a Gaussian size distribution with $\sigma = 15$ for the radius of gyration. Batch processing in the SASfit program (Breßler et al., 2015) was used to compute the fitting for the scattering curves in each pixel. An average real space domain size can be estimated from the radius of gyration, and here an approximation of $R = \sqrt{2}\, R_g$ was applied for estimating the radius of the cross section of thin rods of homogenous density (Hammouda, 2010). To compute the polymorph distribution over the cross section, the peak intensity was extracted of the characteristic peaks at 8.7 nm^{-1} and 9.4 nm^{-1} for the two polymorphic forms I and II (Grzesiak et al., 2003) from each pixel and the ratio between them was plotted in Matlab to generate a map over the polymorphic content.

3. Result and discussion

3.1. Thermal analysis

Thermal analysis was performed to make an initial evaluation of the heterogeneity and solid-state phase of the drug in the solid dispersion.

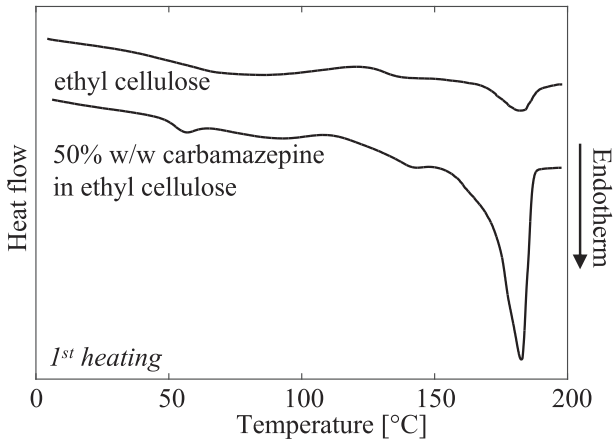

Fig. 2. DSC thermograms of extruded filaments of neat ethyl cellulose and 50% w/w carbamazepine in ethyl cellulose.

Fig. 2 shows the DSC curves from the first heating scans of the dispersion of 50% w/w carbamazepine in ethyl cellulose and the extruded neat ethyl cellulose reference. The second heating scans can be found in the supplementary information (Fig. S3). Ethyl cellulose is a semicrystalline polymer and shows a glass transition at approximately 130 °C and a broad melting endotherm at 180 °C in agreement with previous reports in literature (Mahnaj et al., 2013). The broad endotherms between 60 and 100 °C seen in both extruded samples are attributed to a loss of environmentally absorbed moisture in the extrudate. The thermogram from the carbamazepine in ethyl cellulose dispersion shows two glass transition temperatures at approximately 53 °C and 130 °C, and a broad melting endotherm with onset temperature of 140 °C and peak temperature of 183 °C. The two glass transition temperatures are close to those of neat carbamazepine (56 °C (Li et al., 2000)) and ethyl cellulose (130°), indicating non-mixed carbamazepine and ethyl cellulose. The melting endotherm is found at a temperature around that of neat carbamazepine (in the range 175–190 °C for the four common polymorphs (Pinto et al., 2014) (Fig. S3)) and the melting temperature of ethyl cellulose. The large area of the melting peak indicates a large fraction of crystalline carbamazepine, and the shape of the endotherm shows that there are interactions between the drug and polymer, which both lower and broaden the observed melting endotherm compared to the neat drug polymorphs. Hence, no information on the polymorphic form of the drug crystallites can be derived directly from the thermal response.

3.2. Visualisation and quantification of morphology

Fig. 3 shows the tomography results of the dispersion of carbamazepine in ethyl cellulose with 2D slices extracted from the reconstructed 3D volume perpendicular (Fig. 3a) and parallel (Fig. 3b) to the direction of extrusion. Carbamazepine rich domains with higher electron density show up as bright regions, whereas the ethyl cellulose rich regions show up as dark, i.e., lower density. From these slices it is evident that the dispersion is heterogeneous with the drug mainly distributed over the sample in smaller domains elongated in the extrusion direction with a diameter of just a few 100 nm. In addition, some larger aggregates up to a few microns in size can also be observed. Additional images from the sample volume can be found in the supplementary information (Fig. S4) and a video of the structures throughout consecutive slices (Supp. Video S1).

To quantify the composition of different domains and determine their sizes and connectivity, a segmentation of phases in the sample into different regions is needed. PXCT is a quantitative imaging technique that resolve electron densities, which can be directly correlated to the mass densities with high accuracy when the stoichiometries of the materials are known (Diaz et al., 2012). This makes it intrinsically possible

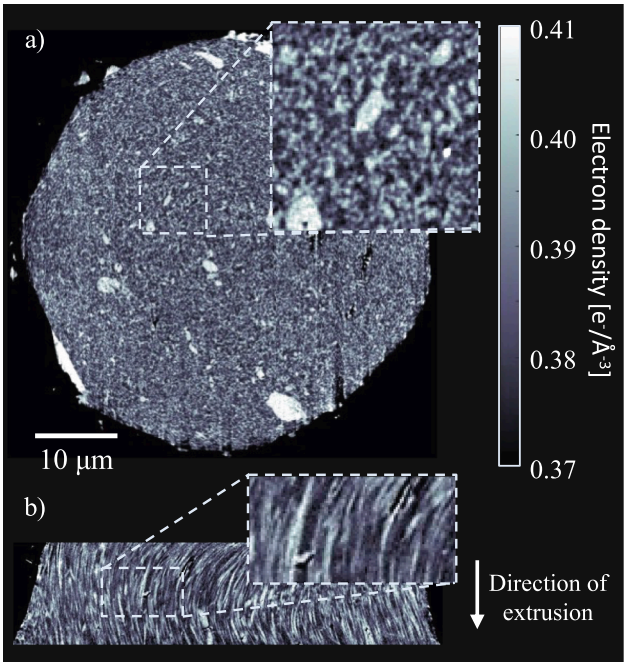

Fig. 3. Tomography slices extracted from the reconstructed 3D volume a) perpendicular and b) parallel to the direction of the extrusion. Brighter regions correspond to carbamazepine rich domains and darker to polymer rich domains.

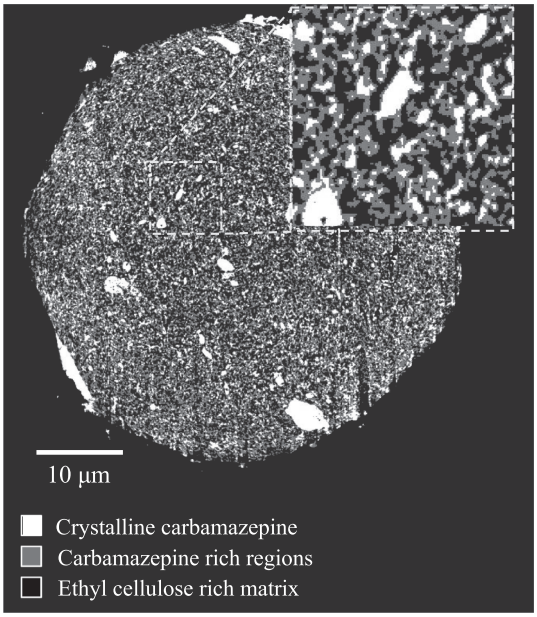

Fig. 4. Segmentation of the three phases in the reconstructed volume of carbamazepine in ethyl cellulose dispersion. Crystalline carbamazepine is shown in white, the ethyl cellulose matrix in black, and the mixed phase of carbamazepine and ethyl cellulose in grey.

to distinguish between different chemical components and between polymorphs based on differences in mass densities. However, the accuracy of the quantitative value within a pixel and the segmentation of a tomography image will always be decided by the data quality in terms of signal to noise ratio and the limits of the resolution compared to the size of the structures in the sample. Discrepancies in the estimated electron density values can therefore arise e.g., if the size of the structures are close to the resolution limit or if there exists unresolved porosity. Therefor the capability of distinguishing between different polymorphs and crystalline and amorphous species are highly sample dependent and diffraction is therefore a suitable complement to more accurately describe the solid-state form of phases present in the sample. In the dispersion used to demonstrate the applicability of PXCT in this study, the domains have similar electron densities and some of the resolved structures have a size close to the resolution limit of the measurement. Therefore, the segmentation was performed with interactive thresholding where the threshold limits were selected both based on electron density values and morphological properties of the distinguishable phases to denote what is determined as crystalline carbamazepine, which can be determined directly from the density differences. Determination between different crystalline polymorphs is instead determined by diffraction as described in section 3.3.

Fig. 4 shows the sample segmented in three phases determined as crystalline carbamazepine, ethyl cellulose rich matrix and a mixed phase denoted as carbamazepine rich regions, which cannot be characterised as either polymer or drug and must therefore consist of a mixture of the two. The segmented crystalline carbamazepine has an average electron density of 0.40 e/Å^{-3} and occupies a volume fraction of 14% in the sample, showing that there is also carbamazepine dispersed in the sample mixed with ethyl cellulose in amorphous form or in crystalline domains below the resolution of the tomography images. The polymer rich matrix has an average density of 0.38 e/Å^{-3}, similar to the reference sample of neat ethyl cellulose (Fig. S5), indicating that the dark matrix mainly consists of drug free polymer. The average electron density of the mixed phase is 0.39 e/Å^{-3}, which is intermediate of the densities of the polymer and crystalline carbamazepine and close to the electron density of amorphous carbamazepine (Grzesiak et al., 2003). This also indicates that this phase consists of either, or both, amorphous carbamazepine and a mixture of the polymer and crystalline carbamazepine. The mixed phase can consist of molecularly dispersed carbamazepine or carbamazepine distributed in domains smaller than the resolution of the experiment. The thermal analysis shows that carbamazepine is present in both amorphous and crystalline form and therefore it is hypothesised that the mixed phase consists of both amorphous and crystalline carbamazepine dispersed in the polymer with a domain size below the resolution of the measurement (80 nm).

Fig. 5 and supplementary Video 2 shows volume renderings of the crystalline carbamazepine and carbamazepine rich regions in the dispersion, visualizing the three-dimensional structure of drug domains. With the 3D images it becomes evident that the elongated domains are not only elongated in the direction of extrusion but also twisted around the centre of the sample in a spiral configuration. This also underlines the importance of three-dimensional imaging for understanding the full morphology in terms of connectivity, tortuosity, and orientation. The oriented spiral pattern is attributed to the shear and elongational forces that the sample is exposed to by the rotating screws and barrel walls during the extrusion process. The formation of oriented structures can further be related to a high melt viscosity of the dispersion due to the high drug concentration and selected processing temperature. The oriented structure also suggests that the phase separated drug domains are present already in the extrusion process and that the high drug concentration hinder the carbamazepine from being fully dispersed in the ethyl cellulose matrix. When the mixture is extruded and cooled down to room temperature, it passes the glass transition temperature of the mixture which locks the structure in place and thus in the previously induced orientation.

3.3. Solid-state phase and domain distribution

To extend the analysis to the full size of the filament and investigate the distribution of nanostructures over the millimetre scale and evaluate the solid-state phase of the drug, scanning S/WAXS were performed on the filaments. Fig. 6a shows WAXS curves selected from two different positions marked in a cross section of the extruded filament in the

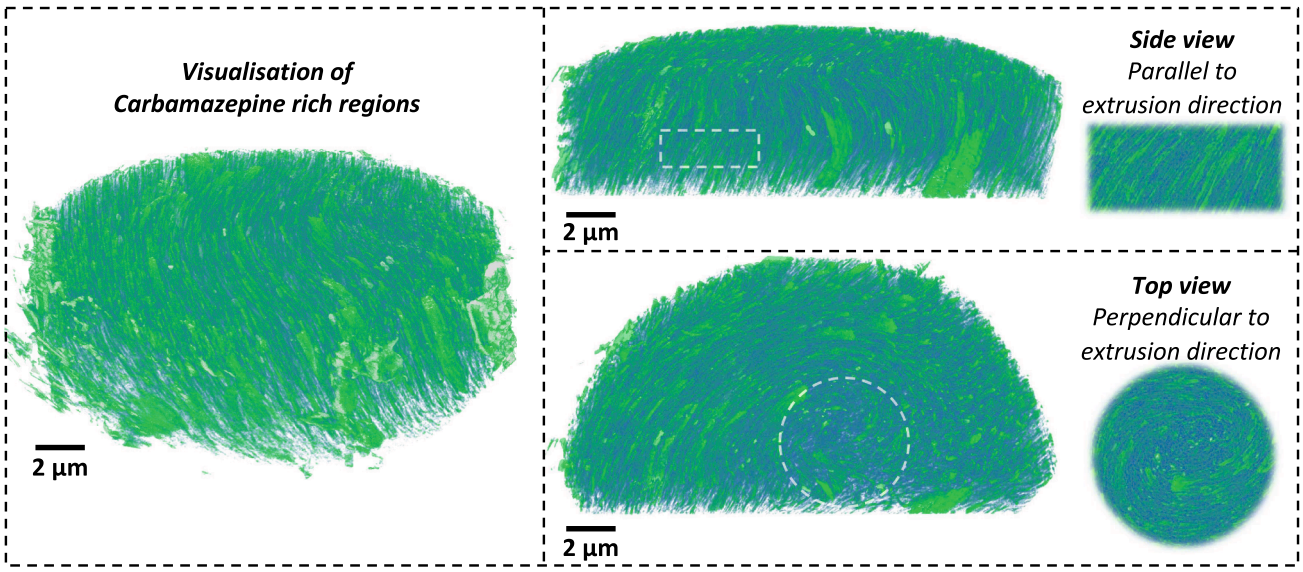

Fig. 5. Volume renderings of the crystalline (lighter green) and carbamazepine rich domains (darker green) in the extruded solid dispersion, constructed from the tomography data. Sub-volumes are shown for ease of interpretation.

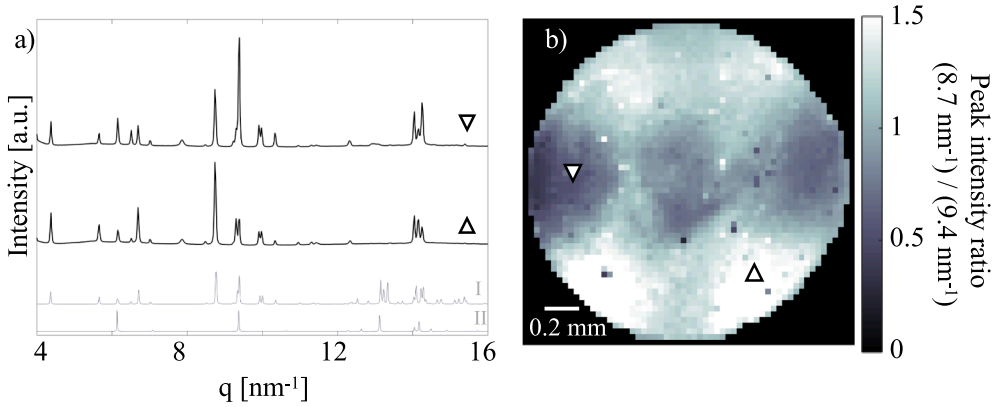

Fig. 6. a) WAXS curves from a sample region of predominately form I (bottom black curve) and from a region where form II dominates (top black curve). Theoretically calculated XRD spectra for the two mentioned polymorphs are shown in grey below the sample curves. b) Scanning WAXS image showing the intensity ratio of the characteristic peaks for form I and II at 8.7 and 9.4 nm^{-1}, respectively, computed in each pixel.

scanning WAXS image in Fig. 6b. The scattering curves show sharp peaks from crystalline carbamazepine on an amorphous background from ethyl cellulose and potential amorphous carbamazepine. An amorphous phase will present a broad, low-intensity scattering curve without the presence of sharp peaks indicating crystallinity in the sample. WAXS therefore has a high detectability for small fractions of crystallinity. Prior to extrusion the carbamazepine powder was in form III, as confirmed with WAXS (Fig. S6), which is the most stable polymorph at room temperature (Grzesiak et al., 2003). The lack of pronounced peaks in the region of 10 to 13.5 nm^{-1} shows that the crystal structure of carbamazepine was transformed from form III into metastable polymorphs during the extrusion process. The WAXS peaks are used to identify the polymorphic content which shows that the crystalline carbamazepine is present as a mixture of mainly two polymorphs, form I and form II. The black bottom curve in Fig. 6a illustrates the WAXS signal from a region dominated by form I, identified by the characteristic peaks at 6.7, 8.7, 9.3, 9.9, and 14.2 nm^{-1} (Grzesiak et al., 2003). The black top curve in Fig. 6a instead shows the WAXS signal from a region dominated by form II with increased intensity of the characteristic peaks at 6.2, 9.4, and 14.3 nm^{-1} (Grzesiak et al., 2003). This means that during the extrusion process the solid-state phase of the carbamazepine changes, either due to melting or dispersion, and the metastable forms I and II are stabilised within the ethyl cellulose matrix at extrusion.

To illustrate the spatial distribution of the polymorphic forms, the ratio between the most pronounced peaks characteristic for each of the two phases, 8.7 and 9.4 nm^{-1}, are plotted for each pixel in Fig. 6b. Regions with higher content of form I are shown in bright and regions with higher content of form II in dark. The cross section of the extruded filament shows different domains dominated by the different polymorphs in a symmetric pattern around the centre of the filament. One explanation for this pattern could be the formation of different flow patterns for different viscosities in different regions of the extruder barrel, caused from an effect of variable heat distribution. It has been shown previously that form I is the most stable polymorph at elevated temperatures, and at temperatures between 160 and 190 °C all polymorphs transform into form I (Grzesiak et al., 2003). A variable heat distribution could therefore explain the heterogeneous distribution of the two polymorphs.

Fig. 7a shows a SAXS curve extracted from the centre of the same cross section measured with WAXS. The SAXS curve shows a broad shoulder in the low q-region centred around 0.025 nm^{-1}. The shoulder is followed by a decay in the intensity proportional to a power law of $q^{-3.7}$ in accordance with Porod's law for surface scattering from nearly

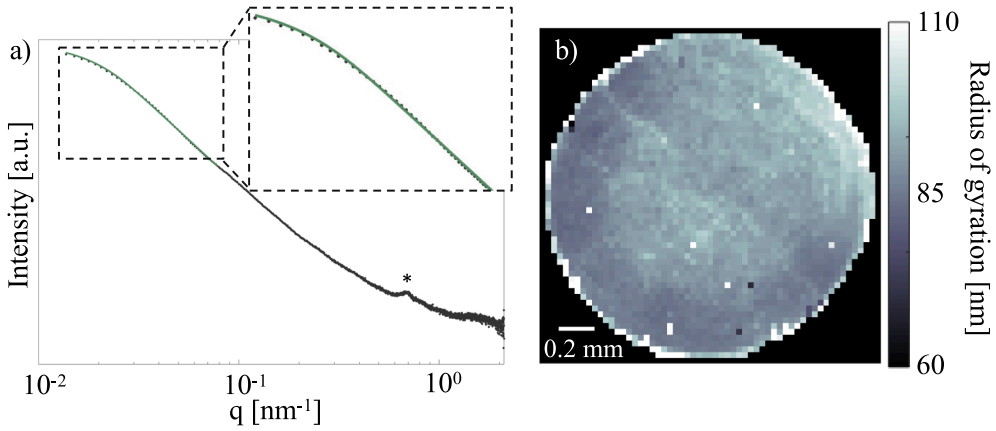

Fig. 7. a) Saxs curve extracted from the centre of the cross section. the curve is fitted with a guinier-porod model to derive a characteristic radius of gyration of carbamazepine domains. b) Scanning saxs image showing the derived radius of gyration, computed in each pixel.

smooth particles (Hammouda, 2010). The shape of the SAXS curves has a high similarity throughout the sample, indicating a similar structure over the cross section of the filament. The peak at 0.67 nm^{-1} corresponds to the epoxy material used for the embedding to cut the thin cross sections and is not related to the structure of a component in the sample.

The shoulder around 0.025 nm^{-1} indicates that there are structures in the sample with a length scale of $\sim 2\pi/0.025\ nm^{-1} = 250$ nm. The PXCT revealed that the crystalline carbamazepine domains are distributed in domains of approximately 250 nm, giving strong support that this shoulder originates from carbamazepine domains. To derive a characteristic domain size from the SAXS curve in each pixel, a Guinier-Porod model was applied to estimate a radius of gyration of the carbamazepine domains. Fig. 7b shows the computed radius of gyration for each scan position over the cross section and reveals minor changes in the radius of gyration with smaller domains towards the edge of the filament. The radius of gyration varies between 80 and 95 nm, which can be converted to a domain size of ~230-270 nm. These results agree well with the structures revealed with tomography where a volume equal to 2 × 2 pixels in the scanning SAXS image is probed. The correlation between the two measurements therefore strongly supports that a morphology similar to the one resolved with tomography (on a 50 μm sample from a filament) can be expected throughout the cross section of the filament and confirms the presence of drug domains with a characteristic size of ~230-270 nm throughout the dispersion. The constant power law decay at higher q shows no direct evidence for smaller domains with a distinct size, favouring the hypothesis that the mixed phase consists of dispersed carbamazepine in ethyl cellulose or amorphous carbamazepine and not crystallites of smaller size than the resolution of the tomography experiment as discussed in section 3.2.

3.4. Orientation analysis

Scanning SAXS is also an efficient method for evaluating structural orientations in a sample. The anisotropy in a two-dimensional scattering pattern is related to sample orientation, making it possible to compute both the preferred angle of oriented structures and its degree of orientation, as a relative measure of the amount of orientation in different parts of the sample. Fig. 8 shows the degree of orientation and the angle of orientation computed for each pixel in the scanning SAXS image perpendicular (top) and parallel (bottom) to the direction of extrusion. The orientations are derived from the asymmetric intensity in the q-range of the shoulder, at 0.014 to 0.050 nm^{-1}, corresponding to the scattering from carbamazepine domains. Fig. 8a shows the degree of orientation where domains with stronger orientation is shown in bright. Fig. 8b shows the angle of orientation in the sample where the orientation angle is illustrated by the hue of the colour wheel and the colour

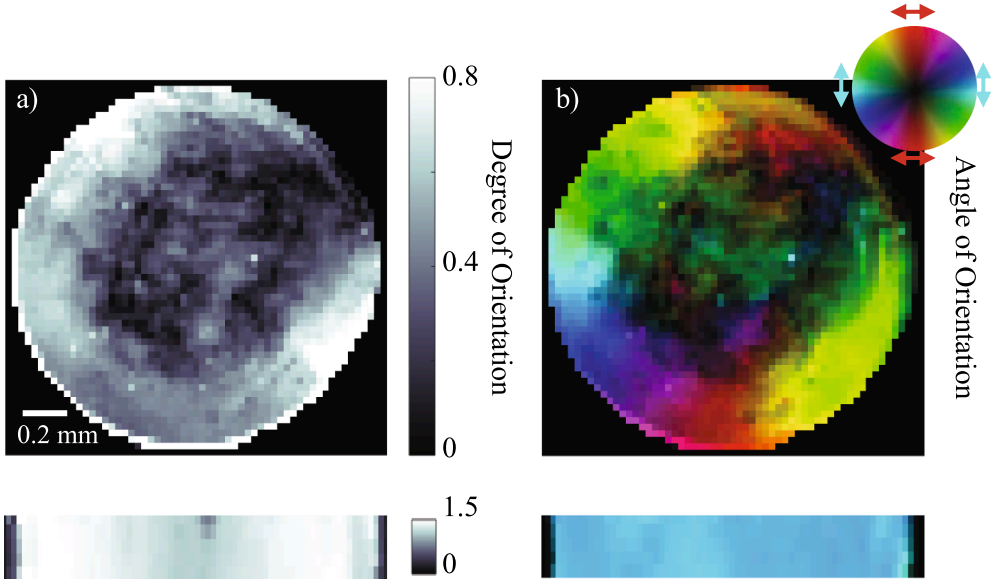

Fig. 8. a) degree of orientation derived from the asymmetry of the saxs pattern, computed in each pixel. higher degree of orientation is shown in bright. b) angle of orientation derived from the preferred orientation of the saxs pattern. the hue of the colour wheel illustrates the angle of orientation, while the intensity of the colour is scaled with the asymmetric scattering intensity, highlighting regions with stronger orientation. the scanning saxs images show the cross-sectional view, perpendicular to the extrusion direction (top), and the parallel view in the direction of extrusion over the intact filament (bottom). orientations are computed in the q-region 0.014 to 0.050 nm^{-1}, corresponding to the scattering from carbamazepine domains.

intensity scales with the asymmetric scattering intensity, highlighting regions with stronger orientation. To guide the eye, arrows are added next to the colour wheel illustrating the conversion of hue to domain orientation.

Fig. 8a shows that the extruded filament has a high degree of orientation of carbamazepine domains in the direction of extrusion (bottom). In the centre of the cross section (top) the degree of orientation is low with higher degree of orientation towards the edge of the filament. Fig. 8b shows that the carbamazepine domains are orientated along the direction of extrusion (bottom) as well as twisted around the centre of the filament (top), similar as the orientations resolved in the nanotomography. However, the low degree of orientation in the centre of the sample contrasts with the nanotomography results that shows a spiral orientation in the centre of the filament. The reason for the discrepancy is attributed to the statistical method of the scattering technique which averages all orientations along the thickness of the sample. The probed sample volume in SAXS is 25^3 μm^3, corresponding to the pixel size times the thickness of the cross section. Within this volume there are multiple changes to the orientation, as can be observed in the volume reconstruction of the carbamazepine domains in Fig. 5, which in SAXS cannot be individually resolved. Therefore, this leads to less asymmetric scattering and a lower degree of orientation. The higher degree of orientation towards the edge of the filament is believed to be a consequence of the shear forces that the mixture is subjected to from the walls of the extruder die, resulting in a stronger more homogenous alignment within a pixel in the sample closer to the extruder walls.

3.5. Application and possibilities for pharmaceutical development.

In the development of solid dosage forms the structure of different components, their domain size and distribution are key for the functioning, physical stability of the compound and for the performance of the drug product. The dissolution properties of the final formulation give phenomenological information but limited knowledge on the origin and the link to structure and morphology. To better understand this, spatially resolved characterisation and imaging can aid to elucidate relations between the structure, morphology and properties and how it connects to the processing. The presented methodology captures two major important characteristics for the analysis of solid dosage forms, spatially resolved characterisation of the morphology and the solid-state phase of the pharmaceutical ingredient. Often pharmaceutical ingredients are polymorphic in nature which can have a strong effect on dissolution rate and hence the absorption rate and bioavailability of the pharmaceutical compounds. Information on the morphology, such as network properties, connectivity and frequency distribution of shape and size of pores and particle sizes can largely impact dissolution and disintegration and provide insights into processibility challenges, if encountered in producing the dosage form. To characterise these properties in depth, the correlative use of imaging and scattering have complementary advantages. Nanotomography provides a direct image of the 3D morphology visualising structures with high resolution in a smaller sub-volume of the sample. On the other hand, scanning S/WAXS efficiently probes nanoscale structures and the solid-state phase over larger regions, generating images with a pixel resolution on the micron scale containing information extracted from the scattering of the sample. By using a correlative approach through the combination of the two techniques, multiscale structural analysis can be conducted, bridging the length scales investigated in the two methods. This can provide essential information of the characteristics of a solid dosage form for pharmaceutical industry and in the development of new pharmaceutical dosage forms.

4. Conclusion

This study introduced a workflow for non-destructive, multiscale characterisation of the structure and morphology of solid dosage forms by combining ptychographic nanotomography and scanning S/WAXS. By using a correlative approach through the combination of the two techniques, multiscale structural analysis was conducted by bridging the length scales investigated in the two methods. The methodology was demonstrated by characterising a hot-melt extruded solid dispersion of carbamazepine in ethyl cellulose which showed a strong link between the distribution of drug domains in the filament and the extrusion process. The results also show a spatial inhomogeneity of different polymorphs of carbamazepine which can be correlated to the extrusion process. This work illustrates how imaging the morphology can enable a better understanding of the origin and formation of structures in solid dosage forms during processing and explain heterogeneous mixtures. By applying the described methodology in the development of pharmaceutical dosage forms, particularly those where the solid-state phase of the drug is critical to performance, a deeper understanding of relationships between processing conditions, morphology, and physical properties of the formulation can be achieved. Upon establishing this, properties of a formulation can be tuned by controlling the morphology of solid dosage forms in the development of new drug delivery systems.

CRediT authorship contribution statement

Martina Olsson: Conceptualization, Methodology, Formal analysis, Investigation, Writing – original draft, Writing – review & editing, Visualization, Funding acquisition. **Rydvikha Govender:** Resources, Writing – review & editing. **Ana Diaz:** Investigation, Writing – review & editing. **Mirko Holler:** Investigation, Writing – review & editing. **Andreas Menzel:** Investigation, Writing – review & editing. **Susanna Abrahmsén-Alami:** Resources, Writing – review & editing. **Matthew Sadd:** Investigation, Writing – review & editing. **Anette Larsson:** Resources, Writing – review & editing. **Aleksandar Matic:** Conceptualization, Methodology, Investigation, Writing – review & editing, Supervision, Funding acquisition. **Marianne Liebi:** Conceptualization, Methodology, Investigation, Writing – review & editing, Supervision, Funding acquisition.

Declaration of Competing Interest

The authors declare that they have no known competing financial interests or personal relationships that could have appeared to influence the work reported in this paper.

Data availability

Data will be made available on request.

Acknowledgements

The authors acknowledge the Paul Scherrer Institute, Villigen PSI, Switzerland for provision of synchrotron radiation beamtime at the beamline cSAXS of the SLS.

Funding

This work was supported by the Area of Advance Nano at Chalmers University of Technology through an excellence initiative PhD student position. The authors acknowledge Vinnova for funding in the program Industrial Pilot Projects (Swedish Innovation Agency VINNOVA 2019-02568). This work was supported by the Chalmers Gender Initiative for Excellence (Genie).

Appendix A. Supplementary data

Supplementary data to this article can be found online at https://doi.org/10.1016/j.ijpharm.2023.123200.

References

Alzahrani, A., Nyavanandi, D., Mandati, P., Youssef, A.A.A., Narala, S., Bandari, S., Repka, M., 2022. A systematic and robust assessment of hot-melt extrusion-based amorphous solid dispersions: Theoretical prediction to practical implementation. Int. J. Pharm. 121951.

Arboleda, C., Lutz-Bueno, V., Wang, Z., Villanueva-Perez, P., Guizar-Sicairos, M., Liebi, M., Varga, Z., Stampanoni, M., 2019. Assessing lesion malignancy by scanning small-angle x-ray scattering of breast tissue with microcalcifications. Phys. Med. Biol. 64 (15), 155010.

Baghel, S., Cathcart, H., O'Reilly, N.J., 2016. Polymeric Amorphous Solid Dispersions: A Review of Amorphization, Crystallization, Stabilization, Solid-State Characterization, and Aqueous Solubilization of Biopharmaceutical Classification System Class II Drugs. J Pharm Sci 105 (9), 2527–2544. https://doi.org/10.1016/j.xphs.2015.10.008.

Baird, J.A., Taylor, L.S., 2012. Evaluation of amorphous solid dispersion properties using thermal analysis techniques. Adv Drug Deliv Rev 64 (5), 396–421. https://doi.org/10.1016/j.addr.2011.07.009.

Breßler, I., Kohlbrecher, J., Thünemann, A.F., 2015. SASfit: a tool for small-angle scattering data analysis using a library of analytical expressions. J. Appl. Cryst. 48 (5), 1587–1598.

Bunk, O., Bech, M., Jensen, T., Feidenhans, R., Binderup, T., Menzel, A., Pfeiffer, F., 2009. Multimodal x-ray scatter imaging. New J. Phys. 11 (12), 123016.

Butreddy, A., Bandari, S., Repka, M.A., 2021. Quality-by-design in hot melt extrusion based amorphous solid dispersions: An industrial perspective on product development. Eur. J. Pharm. Sci. 158, 105655.

Deshmukh, S., Paradkar, A., Abrahmsén-Alami, S., Govender, R., Viridén, A., Winge, F., Matic, H., Booth, J., Kelly, A., 2020. Injection moulded controlled release amorphous solid dispersions: Synchronized drug and polymer release for robust performance. Int. J. Pharm. 575, 118908.

Diaz, A., Trtik, P., Guizar-Sicairos, M., Menzel, A., Thibault, P., Bunk, O., 2012. Quantitative x-ray phase nanotomography. Phys. Rev. B 85 (2), 020104.

Dierolf, M., Menzel, A., Thibault, P., Schneider, P., Kewish, C.M., Wepf, R., Bunk, O., Pfeiffer, F., 2010. Ptychographic X-ray computed tomography at the nanoscale. Nature 467 (7314), 436–439. https://doi.org/10.1038/nature09419.

Duan, P., Lamm, M.S., Yang, F., Xu, W., Skomski, D., Su, Y., Schmidt-Rohr, K., 2020. Quantifying molecular mixing and heterogeneity in pharmaceutical dispersions at sub-100 nm resolution by spin diffusion NMR. Mol. Pharm. 17 (9), 3567–3580.

Fager, C., Barman, S., Roding, M., Olsson, A., Loren, N., von Corswant, C., Bolin, D., Rootzen, H., Olsson, E., 2020a. 3D high spatial resolution visualisation and quantification of interconnectivity in polymer films. Int J Pharm 587, 119622. https://doi.org/10.1016/j.ijpharm.2020.119622.

Fager, C., Roding, M., Olsson, A., Loren, N., von Corswant, C., Sarkka, A., Olsson, E., 2020b. Optimization of FIB-SEM Tomography and Reconstruction for Soft, Porous, and Poorly Conducting Materials. Microsc Microanal 26 (4), 837–845. https://doi.org/10.1017/S1431927620001592.

Florence, A.J., 2010. Polymorph screening in pharmaceutical development. *European Pharmaceutical Review*(4).

Fratzl, P., Jakob, H., Rinnerthaler, S., Roschger, P., Klaushofer, K., 1997. Position-resolved small-angle X-ray scattering of complex biological materials. J. Appl. Cryst. 30 (5), 765–769.

Gamble, J.F., Tobyn, M., Zhang, S., Zhu, A., Šalplachta, J., Matula, J., Zikmund, T., Kaiser, J., Oberta, P., 2021. Characterization of the morphological nature of hollow spray dried dispersion particles using X-ray submicron-computed tomography. AAPS PharmSciTech 23 (1), 40.

Giannini, C., Siliqi, D., Ladisa, M., Altamura, D., Diaz, A., Beraudi, A., Sibillano, T., De Caro, L., Stea, S., Baruffaldi, F., 2014. Scanning SAXS–WAXS microscopy on osteoarthritis-affected bone–an age-related study. J. Appl. Cryst. 47 (1), 110–117.

Govender, R., Abrahmsén-Alami, S., Folestad, S., Larsson, A., 2020. High Content Solid Dispersions for Dose Window Extension: A Basis for Design Flexibility in Fused Deposition Modelling. Pharm. Res. 37 (1), 1–10.

Grzesiak, A.L., Lang, M., Kim, K., Matzger, A.J., 2003. Comparison of the four anhydrous polymorphs of carbamazepine and the crystal structure of form I. J. Pharm. Sci. 92 (11), 2260–2271.

Guizar-Sicairos, M., Diaz, A., Holler, M., Lucas, M.S., Menzel, A., Wepf, R.A., Bunk, O., 2011. Phase tomography from x-ray coherent diffractive imaging projections. Opt. Express 19 (22), 21345–21357.

Habel, H., Andersson, H., Olsson, A., Olsson, E., Larsson, A., Sarkka, A., 2016. Characterization of pore structure of polymer blended films used for controlled drug release. J Control Release 222, 151–158. https://doi.org/10.1016/j.jconrel.2015.12.011.

Hammouda, B., 2010. A new Guinier-Porod model. J. Appl. Cryst. 43 (4), 716–719.

Holler, M., Raabe, J., Wepf, R., Shahmoradian, S.H., Diaz, A., Sarafimov, B., Lachat, T., Walther, H., Vitins, M., 2017. OMNY PIN—A versatile sample holder for tomographic measurements at room and cryogenic temperatures. Rev. Sci. Instrum. 88 (11), 113701.

Holler, M., Raabe, J., Diaz, A., Guizar-Sicairos, M., Wepf, R., Odstrcil, M., Shaik, F.R., Panneels, V., Menzel, A., Sarafimov, B., Maag, S., Wang, X., Thominet, V., Walther, H., Lachat, T., Vitins, M., Bunk, O., 2018. OMNY-A tOMography Nano crYo stage. Rev Sci Instrum 89 (4), 043706. https://doi.org/10.1063/1.5020247.

Holler, M., Ihli, J., Tsai, E.H.R., Nudelman, F., Verezhak, M., van de Berg, W.D.J., Shahmoradian, S.H., 2020. A lathe system for micrometre-sized cylindrical sample preparation at room and cryogenic temperatures. J Synchrotron Radiat 27 (Pt 2), 472–476. https://doi.org/10.1107/S1600577519017028.

Howells, M.R., Beetz, T., Chapman, H.N., Cui, C., Holton, J., Jacobsen, C., Kirz, J., Lima, E., Marchesini, S., Miao, H., 2009. An assessment of the resolution limitation due to radiation-damage in x-ray diffraction microscopy. J. Electron Spectrosc. Relat. Phenom. 170 (1–3), 4–12.

Koivunotko, E., Merivaara, A., Niemela, A., Valkonen, S., Manninen, K., Makinen, H., Viljanen, M., Svedstrom, K., Diaz, A., Holler, M., 2021. Molecular insights on successful reconstitution of freeze-dried nanofibrillated cellulose hydrogel. ACS Applied Bio Materials 4 (9), 7157–7167.

Lefort, R., De Gusseme, A., Willart, J.-F., Danede, F., Descamps, M., 2004. Solid state NMR and DSC methods for quantifying the amorphous content in solid dosage forms: an application to ball-milling of trehalose. Int. J. Pharm. 280 (1–2), 209–219.

Li, Y., Han, J., Zhang, G.G., Grant, D.J., Suryanarayanan, R., 2000. In situ dehydration of carbamazepine dihydrate: A novel technique to prepare amorphous anhydrous carbamazepine. Pharm. Dev. Technol. 5 (2), 257–266.

Liu, H., Taylor, L.S., Edgar, K.J., 2015. The role of polymers in oral bioavailability enhancement; a review. Polymer 77, 399–415.

Luebbert, C., Klanke, C., Sadowski, G., 2018. Investigating phase separation in amorphous solid dispersions via Raman mapping. Int J Pharm 535 (1–2), 245–252. https://doi.org/10.1016/j.ijpharm.2017.11.014.

Mahnaj, T., Ahmed, S.U., Plakogiannis, F.M., 2013. Characterization of ethyl cellulose polymer. Pharm. Dev. Technol. 18 (5), 982–989.

Marucci, M., Andersson, H., Hjartstam, J., Stevenson, G., Baderstedt, J., Stading, M., Larsson, A., von Corswant, C., 2013. New insights on how to adjust the release profile from coated pellets by varying the molecular weight of ethyl cellulose in the coating film. Int J Pharm 458 (1), 218–223. https://doi.org/10.1016/j.ijpharm.2013.09.016.

Merivaara, A., Kekkonen, J., Monola, J., Koivunotko, E., Savolainen, M., Silvast, T., Svedström, K., Diaz, A., Holler, M., Korhonen, O., 2022. Near-infrared analysis of nanofibrillated cellulose aerogel manufacturing. Int. J. Pharm. 617, 121581.

Nielsen, M.S., Munk, M.B., Diaz, A., Pedersen, E.B.L., Holler, M., Bruns, S., Risbo, J., Mortensen, K., Feidenhans, R., 2016. Ptychographic X-ray computed tomography of extended colloidal networks in food emulsions. Food Struct. 7, 21–28.

Odstrčil, M., Holler, M., Raabe, J., Guizar-Sicairos, M., 2019a. Alignment methods for nanotomography with deep subpixel accuracy. Opt. Express 27 (25), 36637–36652.

Odstrčil, M., Lebugle, M., Guizar-Sicairos, M., David, C., Holler, M., 2019b. Towards optimized illumination for high-resolution ptychography. Opt. Express 27 (10), 14981–14997.

Pandi, P., Bulusu, R., Kommineni, N., Khan, W., Singh, M., 2020. Amorphous solid dispersions: An update for preparation, characterization, mechanism on bioavailability, stability, regulatory considerations and marketed products. Int. J. Pharm. 586, 119560.

Pfeiffer, F., 2018. X-ray ptychography. Nat. Photonics 12 (1), 9–17.

Pindelska, E., Szeleszczuk, L., Pisklak, D.M., Mazurek, A., Kolodziejski, W., 2015. Solid-state NMR as an effective method of polymorphic analysis: Solid dosage forms of clopidogrel hydrogensulfate. J. Pharm. Sci. 104 (1), 106–113.

Pinto, M.A.L., Ambrozini, B., Ferreira, A.P.G., Cavalheiro, É.T.G., 2014. Thermoanalytical studies of carbamazepine: hydration/dehydration, thermal decomposition, and solid phase transitions. Braz. J. Pharm. Sci. 50, 877–884.

Purohit, H.S., Ormes, J.D., Saboo, S., Su, Y., Lamm, M.S., Mann, A.K.P., Taylor, L.S., 2017. Insights into Nano- and Micron-Scale Phase Separation in Amorphous Solid Dispersions Using Fluorescence-Based Techniques in Combination with Solid State Nuclear Magnetic Resonance Spectroscopy. Pharm Res 34 (7), 1364–1377. https://doi.org/10.1007/s11095-017-2145-z.

Purohit, H.S., Taylor, L.S., 2015. Miscibility of Itraconazole-Hydroxypropyl Methylcellulose Blends: Insights with High Resolution Analytical Methodologies. Mol Pharm 12 (12), 4542–4553. https://doi.org/10.1021/acs.molpharmaceut.5b00761.

Purohit, H.S., Taylor, L.S., 2017. Phase Behavior of Ritonavir Amorphous Solid Dispersions during Hydration and Dissolution. Pharm Res 34 (12), 2842–2861. https://doi.org/10.1007/s11095-017-2265-5.

Repka, M.A., Bandari, S., Kallakunta, V.R., Vo, A.Q., McFall, H., Pimparade, M.B., Bhagurkar, A.M., 2018. Melt extrusion with poorly soluble drugs–An integrated review. Int. J. Pharm. 535 (1–2), 68–85.

Rodriguez-Palomo, A., Lutz-Bueno, V., Cao, X., Kádár, R., Andersson, M., Liebi, M., 2021. In situ visualization of the structural evolution and alignment of lyotropic liquid crystals in confined flow. Small 17 (7), 2006229.

Rumondor, A.C., Ivanisevic, I., Bates, S., Alonzo, D.E., Taylor, L.S., 2009. Evaluation of drug-polymer miscibility in amorphous solid dispersion systems. Pharm. Res. 26, 2523–2534.

Rumondor, A.C., Taylor, L.S., 2010. Effect of polymer hygroscopicity on the phase behavior of amorphous solid dispersions in the presence of moisture. Mol. Pharm. 7 (2), 477–490.

Sanabria Ortiz, K., Hernández Espinell, J.R., Ortiz Torres, D., Lopez-Mejias, V., Stelzer, T., 2019. Polymorphism in solid dispersions. Cryst. Growth Des. 20 (2), 713–722.

Schittny, A., Huwyler, J., Puchkov, M., 2020. Mechanisms of increased bioavailability through amorphous solid dispersions: a review. Drug Deliv. 27 (1), 110–127.

Takeuchi, I., Shimakura, K., Kuroda, H., Nakajima, T., Goto, S., Makino, K., 2015. Estimation of crystallinity of nifedipine–polyvinylpyrrolidone solid dispersion by usage of terahertz time-domain spectroscopy and of X-ray powder diffractometer. J. Pharm. Sci. 104 (12), 4307–4313.

Thibault, P., Dierolf, M., Bunk, O., Menzel, A., Pfeiffer, F., 2009. Probe retrieval in ptychographic coherent diffractive imaging. Ultramicroscopy 109 (4), 338–343. https://doi.org/10.1016/j.ultramic.2008.12.011.

Thibault, P., Guizar-Sicairos, M., 2012. Maximum-likelihood refinement for coherent diffractive imaging. New J. Phys. 14 (6), 063004.

Tian, B., Tang, X., Taylor, L.S., 2016. Investigating the Correlation between Miscibility and Physical Stability of Amorphous Solid Dispersions Using Fluorescence-Based

Techniques. Mol Pharm 13 (11), 3988–4000. https://doi.org/10.1021/acs.molpharmaceut.6b00803.
Tiwari, R.V., Patil, H., Repka, M.A., 2016. Contribution of hot-melt extrusion technology to advance drug delivery in the 21st century. Expert Opin. Drug Deliv. 13 (3), 451–464.
van Heel, M., Schatz, M., 2005. Fourier shell correlation threshold criteria. J Struct Biol 151 (3), 250–262. https://doi.org/10.1016/j.jsb.2005.05.009.
Vijayakumar, J., Goudarzi, N.M., Eeckhaut, G., Schrijnemakers, K., Cnudde, V., Boone, M.N., 2023. Characterization of Pharmaceutical Tablets by X-ray Tomography. Pharmaceuticals 16 (5), 733.
Wakonig, K., Stadler, H.C., Odstrcil, M., Tsai, E.H.R., Diaz, A., Holler, M., Usov, I., Raabe, J., Menzel, A., Guizar-Sicairos, M., 2020. PtychoShelves, a versatile high-level framework for high-performance analysis of ptychographic data. J Appl Crystallogr 53 (Pt 2), 574–586. https://doi.org/10.1107/S1600576720001776.
Yamamoto, E., Takeda, Y., Ando, D., Koide, T., Amano, Y., Miyazaki, S., Miyazaki, T., Izutsu, K.-I., Kanazawa, H., Goda, Y., 2021. Discrimination of ranitidine hydrochloride crystals using X-ray micro-computed tomography for the evaluation of three-dimensional spatial distribution in solid dosage forms. Int. J. Pharm. 605, 120834.